Glass-Glass Transitions by Means of an Acceptor-Donor Percolating Electric-Dipole Network

Le Zhang,[1,2,*] Xiaojie Lou,[1] Dong Wang,[1,†] Yan Zhou,[3] Yang Yang,[1]
Martin Kuball,[3] Michael A. Carpenter,[2] and Xiaobing Ren[1,4,‡]

[1]*Multidisciplinary Materials Research Center and Center for Microstructure Science, Frontier Institute of Science and Technology and State Key Laboratory for Mechanical Behavior of Materials, Xi'an Jiaotong University, Xi'an 710054, China*
[2]*Department of Earth Sciences, University of Cambridge, Downing Street, Cambridge CB2 3EQ, United Kingdom*
[3]*Center for Device Thermography and Reliability, H. H. Wills Physics Laboratory, University of Bristol, Bristol BS8 1TL, United Kingdom*
[4]*Ferroic Physics Group, National Institute for Materials Science, Tsukuba 305-0047, Ibaraki, Japan*

(Received 26 April 2017; revised manuscript received 9 August 2017; published 9 November 2017; corrected 1 February 2018)

We report the ferroelectric glass-glass transitions in $KN(K^+/Nb^{5+})$-doped $BaTiO_3$ ferroelectric ceramics, which have been proved by x-ray diffraction profile and Raman spectra data. The formation of glass-glass transitions can be attributed to the existence of cubic (C)-tetragonal (T)-orthorhombic (O)-rhombohedral (R) ferroelectric transitions in short-range order. These abnormal glass-glass transitions can perform very small thermal hysteresis (approximately 1.0 K) with a large dielectric constant (approximately 3000), small remanent polarization P_r, and relative high maximum polarization P_m remaining over a wide temperature range (220–350 K) under an electrical stimulus, indicating the potential applications in dielectric recoverable energy-storage devices with high thermal reliability. Further phase field simulations suggest that these glass-glass transitions are induced by the formation of a percolating electric defect-dipole network (PEDN). This proper PEDN breaks the long-range ordered ferroelectric domain pattern and results in the local phase transitions at the nanoscale. Our work may further stimulate the fundamental physical theory and accelerate the development of dielectric energy-storing devices.

DOI: 10.1103/PhysRevApplied.8.054018

I. INTRODUCTION

Dielectric materials play an important role in the storage of electric powers due to their fast response of polarization by an applied external electric field, which makes them potential applications for power pulse devices, multilayer ceramic capacitors, hybrid electric vehicles, and portable electronic devices [1–5]. However, the low permittivity, low breakdown strength, high hysteresis loss, and narrow temperature range of current lead-free environmental-friendly dielectric materials result in low-energy density and efficiency and will limit their applications [3,4,6,7]. Previously, giant dielectric properties with low hysteresis have been reported in the lead-based relaxor ferroelectrics (ferroelectric glass) region of $Pb(Mg_xNb_{1-x})O_3$ [8–11], which suggests to us that relaxor ferroelectrics seem to be a potential way to solve some of the problems above [3,12].

The relaxor ferroelectric is one important part of ferroic glass families including relaxor in ferroelectric systems, spin glass in ferromagnetic systems, and strain glass in ferroelastic systems, which are all normally understood by the appearance of nanocaled ferroic domains caused by doping proper point defects [13,14]. These ferroic glass transitions can result in proper dielectric, magnetic, and enhanced mechanical behaviors with a low hysteresis in a wide frequency or temperature range [8,13,15]. For relaxor ferroelectrics, their main characteristic is the existence of polar nanoregions (PNRs) [8]. The origin of giant dielectric and electrostrictive properties with low hysteresis is mostly considered as the easy polarization rotation or significant growth of ferroelectic nanodomains under the external electric field [8].

On the other hand, phase transitions between ferroelectric phases, e.g., the morphotropic phase boundary (MPB) composition in ferroelectric and piezoelectric compounds [e.g., $Pb(Zr_{1-x}Ti_x)O_3$], can exhibit some excellent properties like dielectric permittivity, piezoelectricity, and electrostrain, which have made them the critical component for state-of-the-art piezoelectric sensors and actuators [9–11,16–18]. This can be attributed to the existence of a more flattened free energy profile, which results in a structure instability among different states and is also quite sensitive to an external electric field [10,11,17–22]. However, this MPB composition shows large remanent polarization P_r and large maximum polarization P_m at the

*Corresponding author.
zhangleking005@gmail.com
†Corresponding author.
wang_dong1223@xjtu.edu.cn
‡Corresponding author.
Ren.xiaobing@xjtu.edu.cn

same time accompanying a narrow temperature range in lead-free systems, which limits the energy storage efficiency and applicable temperature range.

The study of lead-free dielectric materials with a higher dielectric permittivity, lower hysteresis, lower remanent polarization, and higher maximum polarization over a wide temperature range should be the requirements of the next generation of energy-storage device. It may be solved by combining MPB-like phase diagrams with relaxor ferroelectrics (FE) transitions, which could have both large dielectric properties, low hysteresis, low P_r, and high P_m. Previous results have reported the possibility by integrating the properties of both a long-range order FE transition and relaxor transitions, which show high piezoelectric or dielectric properties [10,11]. However, no work has reported the integrating of two glass transitions (relaxor ferroelectrics) in ferroelectrics, especially in lead-free substances. It also remains a mystery how to design such a glass-glass transition and whether this special state could improve the dielectric energy-storage properties or perform other interesting properties.

In this work, we reported the tetragonal (T)-orthorhombic (O)-rhombohedral (R) glass-glass transitions in $BaTiO_3$ (BTO) ceramics codoped with K^+ and Nb^{5+}, abbreviated as BT-xKN (x is the mole percent of $KNbO_3$). The glass-glass transitions can effectively decrease the thermal hysteresis with a minimal value of 0.7–1.2 K and perform dielectric constants about 3000, which is higher than the ambient dielectric performance (permittivity of 500–1500) of many lead-free ferroelectrics [7]. Specially, a small remanent polarization P_r and relatively large maximum polarization P_m over a wide temperature range (220–350 K) have been found, which indicates the potential application in dielectric energy-storing devices with high thermal reliability and sensitivity. Our phase field simulations find that this glass-glass transition can be induced by the formation of a percolating electric-dipole network (PEDN) caused by doped point defects. This proper PEDN breaks or confines the formation of a long-range ordered ferroelectric domain pattern and results in local phase transitions at the nanoscale.

II. EXPERIMENTAL METHODS

BT-xKN (x is the mole percent of $KNbO_3$) is fabricated by a conventional solid-state reaction method with starting chemicals of K_2CO_3 (99.8%), Nb_2O_5 (99.9%), $BaCO_3$ (99.95%), and TiO_2 (99.9%). The calcining of all samples is performed at 1473 K for 3 h, and sintering is done at 1553–1573 K for 3 h in the air. A and B sites of $BaTiO_3$ can be doped by K^+ and Nb^{5+} cations, respectively. The opposing faces of the sample disk are coated with silver, and the temperature dependence of the permittivity, ε_r, is determined by using a HIOKI 3532 LCR meter with testing frequencies of 0.1, 1, 10, 100, and 300 kHz. The disk is then sewn up and used for the measurement of heat flow by differential scanning calorimetry (DSC) with a cooling and heating rate of 10 K/ min. Raman spectra are carried out with a changing temperature range from 473 to 133 K in the frequency range from 50 to 800 cm^{-1}.

III. RESULTS

Figure 1 shows the dielectric permittivity and heat flow data by LCR and DSC for BTO and BT-1KN ceramics, respectively. The detected temperature anomalies in Fig. 1 correspond to phase transitions of BTO and BT-1KN which are consistent with previous work [23]. We can clearly see the typical ferroelectric phase transition signals of $BaTiO_3$ (long-range order to long-range order) from three sharp dielectric peaks [Fig. 1(a)] and heat flow peaks [C-T (at 398 K), T-O (at 281 K), and O-R (at 189 K)] [Fig. 1(b)]. The transition temperatures of T-O or O-R for BT-1KN ceramics from the dielectric permittivity data [Fig. 1(c)] do not change with frequency. But the dielectric value under different frequencies indeed changes. Furthermore, different from the results of pure BTO, the signals of T-O and O-R transitions in BT-1KN become broad for dielectric measurement, and the heat flow peaks are nearly vanished in DSC signals [Fig. 1(d)]. This can be attributed to the appearance of some local strain field caused by dopants, which smear the transition temperatures [24]. Furthermore, our results show that the T-O and O-R phase transition temperatures both increase and T_c decreases with the increase of KN dopant composition (from $x = 0$ to $x = 1$), which seems to be inclined to form a phase-convergence region.

When the composition of KN is close to $x = 2$, the signal of ferroelectric phase transitions of BTO, C-T, T-O, and O-R, suddenly vanishes in the DSC heat flow curve, as

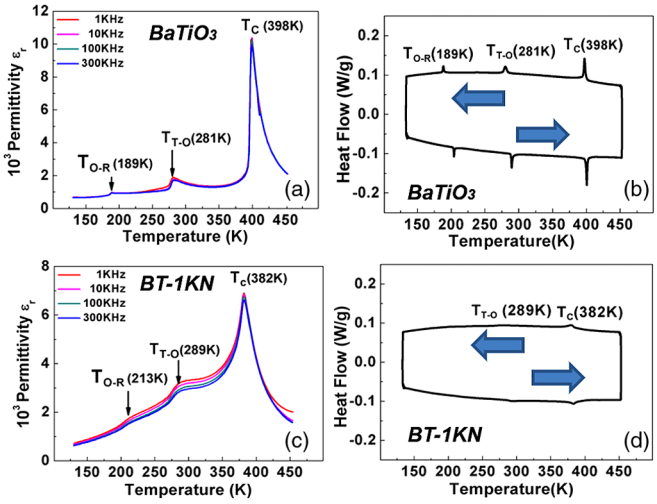

FIG. 1. (a) Dielectric permittivity upon cooling with a frequency of 1, 10, 100, and 300 kHz for pure $BaTiO_3$. (b) DSC heat flow curve of pure BTO upon cooling and heating. (c) Dielectric permittivity upon cooling with a frequency of 1, 10, 100, and 300 kHz for BT-1KN. (d) DSC heat flow curve of BT-1KN.

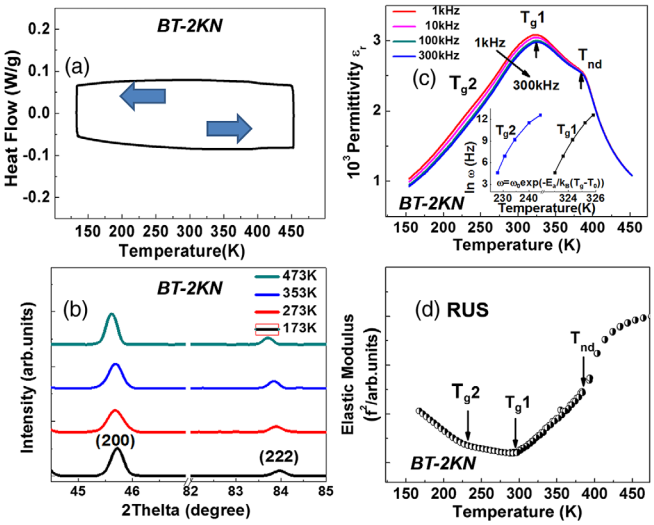

FIG. 2. (a) DSC heat flow curve for BT-2KN. (b) XRD profiles at different temperatures for BT-2KN. (c) Dielectric permittivity data with a frequency of 1, 10, 100, and 300 kHz for BT-2KN, T_{nd} is the start temperature of nanodomain formation, T_{g1} and T_{g2} describe the two glass transition temperatures, respectively, and the inset figure describes the Vogel-Fulcher relationship for T_{g1} and T_{g2}. (d) The elastic modulus change of BT-2KN upon cooling from RUS measurement.

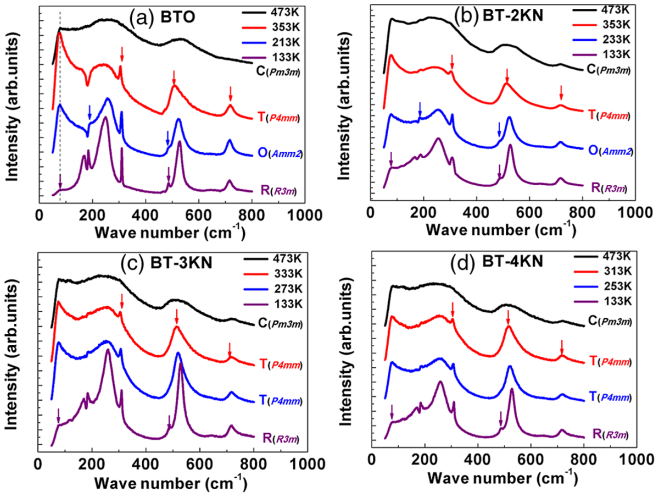

FIG. 3. The Raman spectra at different temperatures in (a) $BaTiO_3$, (b) BT-2KN, (c) BT-3KN, and (d) BT-4KN. The characteristic spectrum of cubic (*Pm3m*), tetragonal (*P4mm*), orthorhombic (*Amm2*), and rhombohedral (*R3m*) phases are labeled.

shown in Fig. 2(a) (BT-2KN). The temperature evolution of XRD profiles [Fig. 2(b)] clearly confirms that the structure of BT-2KN still remains cubic (no peak splitting) upon cooling from above T_c to 133 K. Generally, such a phenomenon can be explained by two possibilities: (i) a nontransforming region or (ii) a glass region by ferroic glass transitions [13–15]. In order to clarify this, the dielectric permittivity and elastic modulus upon cooling are measured in order to capture the information of glass transitions [shown in Figs. 2(c) and 2(d)], and the local structure changes are measured by Raman spectra, shown in Fig. 3.

The dielectric permittivity (ε_r) vs temperature (T) data of BT-2KN sample at different frequencies (1 kHz to 300 kHz) is shown in Fig. 2(c). The results show three characteristic temperatures with frequency dispersion, T_{nd}(~387 K), T_{g1}(~323 K), and T_{g2}(~218 K), which reveal the existence of three special transitions. They are distinctly different from the normal ferroelectric phase transition behaviors in the pure $BaTiO_3$ characterized by a sharp peak with frequency independence [Fig. 1(a)]. The frequency-dependent behavior around T_{g1} and T_{g2} can be fitted by using a non-Arrhenius dependence, i.e., the empirical Vogel-Fulcher law $\omega = \omega_{0*}\exp[-E_a/k_B(T_g - T_0)]$, shown as an inset in Fig. 2(c)[25]. The best fitting of T_{g1} and T_{g2} confirms the existence of glass transitions. The fitting result of T_{g1} shows E_a (activation energy) approximately 0.01 eV, $\omega_0 \sim 10^{12}$ s^{-1}, $T_0 \sim 318$ K, and $T_{g1}/T_0 \sim 1.03$, where T_0 is called the "ideal glass-glass" transition temperature. To obtain the accurate value of T_{g2}, we do a second-order derivative of the dielectric permittivity and get the accurate values of T_{g2} under different frequencies. The fitting results of T_{g2} show $E_a \sim 0.023$ eV, $\omega_0 \sim 10^9$ s^{-1}, $T_0 \sim 211.55$ K, and $T_{g2}/T_0 \sim 1.16$. The different activation energy and relaxation time at T_{g1} and T_{g2} from the Vogel-Fulcher fitting suggest that the two glass transitions are different.

The three anomaly temperatures of BT-2KN can further be observed and evidenced in elastic moduli vs temperature curves by resonant ultrasound spectroscopy (RUS) measurements [Fig. 2(d)]. f^2 obtained from RUS is effectively proportional to the shear modulus. The continuous softening and hardening of the modulus exhibits two modulus dips at phase transition temperatures T_{g1} and T_{g2} upon cooling, shown by the arrows in Fig. 2(d), which indicates the two-step FE glass-glass transitions accompanying the structure change [26–30].

In order to gain detailed insight into the local structure of these glass transition regions, the Raman spectra at different temperatures for BT-2KN are detected. As a phonon detective measurement, Raman spectroscopy has a higher resolution for the nanosized ferroelectric phase transition than x-ray diffraction [31]. The Raman spectra of BT-2KN, obtained at 473 K (above T_{nd}), 353 K (between T_{nd} and T_{g1}), 233 K (between T_{g1} and T_{g2}), and 133 K (below T_{g2}), are displayed in Fig. 3(b), where all spectra of BT-2KN are consistent with the characteristics of the transverse (TO) and longitudinal (LO) optical modes in BTO, i.e., approximately 185 cm^{-1} (TO), approximately 250 cm^{-1} (LO), approximately 310 cm^{-1} (LO and TO), approximately 525 cm^{-1} (TO), and approximately 715 cm^{-1} (LO), indicating a perovskite structure [31–34].

TABLE I. The characteristic Raman mode for different symmetries in pure BTO and BT-2KN ceramics.

Raman mode								
Local structure	~80	165	~185	~250	~310	~485	~525	~715
Cubic				Weak			Weak	
Tetragonal	√	Weak		Weak	√		√	√
Orthorhombic	√	Weak	√	√	√	√	√	√
Rhombohedral		√	√	√	√	√	√	√

For comparison, Fig. 3(a) shows the phonon vibration mode characteristics of different phases in pure BTO ($x = 0$), e.g., cubic (at 473 K), tetragonal (at 353 K), orthorhombic (at 213 K), and rhombohedral (at 133 K) [31–34], including the disappearance or appearance of Raman modes as shown in Table I. Based on the results in BTO, the different local structures of BT-2KN have been characterized by different mode behavior and marked by arrows in Fig. 3(b): cubic (high half-width of all phonon modes) at 473 K, tetragonal [appearance of approximately 80 cm^{-1}, 310 cm^{-1} (LO and TO), 525 cm^{-1} (TO), and approximately 715 cm^{-1} (LO)] at 353 K, orthorhombic [appearance of approximately 185 cm^{-1} (TO) and approximately 485 cm^{-1} (TO)] at 233 K, rhombohedral [disappearance of approximately 80 cm^{-1} and appearance of approximately 165 cm^{-1} (TO)] at 133 K. Therefore, our results confirm the existence of a local structure change from *C* to *T* to *O* to *R* upon cooling at $x = 2$. The observed three glass-glass transitions at T_{g1} and T_{g2} in Fig. 2 should correspond to *T*-*O* and *O*-*R* glass-glass transitions, respectively.

From the temperature evolution of Raman spectra $x = 3$ [Fig. 3(c)] and $x = 4$ [Fig. 3(d)], the characteristics of orthorhombic structure do not appear, however, i.e., the disappearance of the approximately 485 cm^{-1} (TO) mode and the silence of the approximately 185 cm^{-1} (TO) mode. It indicates that the tetragonal phase directly transforms to the rhombohedral without the appearance of a stable orthorhombic phase. From Fig. 3, we can see the mode of 165, 185, and 310 cm^{-1} become more silent upon cooling with increasing the doping KN composition, no peak shift, or a peak width change. It is different from the pure BTO case, indicating that the domain size becomes smaller and smaller with increasing the KN doping composition to $x = 2\%$–4%. It is considered as the glass transition characteristics.

Based on the temperature dependencene of the Raman spectra of BTO and BT-2KN [partly shown Figs. 3(a) and 3(b), respectively] between 133 and 473 K, the temperature evolution of one longitudinal optical mode (LO, approximately 250 cm^{-1}) and one transverse optical mode (TO, approximately 525 cm^{-1}) are investigated in detail, including the frequency shift and half-width of these modes. Figures 4(a) and 4(b) show the data of the 250 cm^{-1} LO mode in BTO and BT-2KN compositions, respectively. Their left red axis is the temperature dependence of frequency, and the right is related to the half-width. This LO mode is very sensitive to the ferroelectric transitions in BTO rather than the glass-glass transitions in BT-2KN. The sharp frequency shifts with changing temperatures shown in Fig. 4(a) correspond to the *C*-*T* (approximately 393 K), *T*-*O* (283 K), and *O*-*R* (193 K) transitions of BTO, respectively. The half-width change of this mode upon cooling seems to be nonsensitive to the ferroelectric phase transitions, although two very weak dips appear at *T*-*O* and *O*-*R* transitions. While the composition around $x = 2$, all frequency dips of 250 cm^{-1} [Fig. 4(b)] are broad and weak at glass-glass transitions, which is considered as the characteristics of glass states. However, the *C*-*T* glass transitions can also be clearly observed from Fig. 4(b). It indicates that the distortion change of *T*-*O* or *O*-*R* glass-glass transitions is much weaker. It is consistent with the results that show no average structure change in the XRD data.

Another characteristic TO mode around 525 cm^{-1} is also investigated in BTO and BT-2KN as shown in Figs. 4(c) and 4(d), respectively. This frequency shift and half-width of this TO mode seem to be sensitive to the *C*-*T* transition of BTO and BT-2KN both rather than the *T*-*O* and *O*-*R* transitions. Indeed, very weak anomalies around 283 and

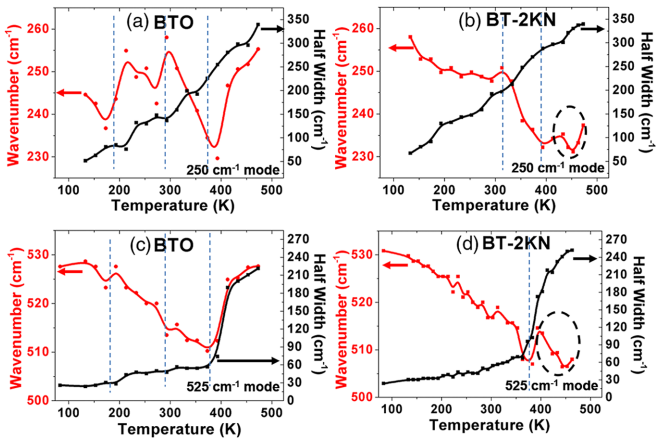

FIG. 4. (a),(b) Temperature evolution of the frequency (red left axis) and half-width (black right axis) of an approximately 250 cm^{-1} (LO) mode in BTO and BT-2KN, respectively; (c), (d) the temperature vs frequency (red left axis) and half-width (black right axis) of an approximately 525 cm^{-1} (TO) mode in BTO and BT-2KN.

190 K can be discovered in BTO, which can be considered as the T-O and O-R transitions. However, this phenomena is not clearly discovered in the BT-2KN. It is consistent with the physics of the 250 cm^{-1} mode, indicating a nanoscale structure transition without an average microscale structure change in BT-2KN.

IV. DISCUSSIONS

Based on our findings, the complete phase diagram of the BT-xKN ($0 < x < 8$) system is established in Fig. 5(a). This phase diagram shows unusual characteristics around $x = 1.5$, separating the regular ferroelectric phase transition region ($x < 1.5$) from the ferroelectric glass-glass transition (relaxor-relaxor) segment ($x > 1.5$). The normal ferroelectric phase transition sequence of $BaTiO_3$ (C-T-O-R) can be changed to abnormal cubic-T glass-O glass-R glass phase transition order at $x = 2$. With the increase of the KN composition (e.g., $x \geq 3$), a T glass-R glass ($x = 3$–5) phase transition is discovered, and $x = 3$ is the coexistence point of the three-glasses state. The composition-dependent permittivity and hysteresis results around the T-O or T-R transition temperature (maximum of dielectric permittivity, T_m), shown in Fig. 5(b). It demonstrates that the T-O or T-R glass-glass transitions can exhibit very low hysteresis with high permittivity, especially at the three-glasses coexistence point ($x = 3$, 298 K), which performs the lowest hysteresis (approximately 0.7 K) with the highest permittivity (approximately 3100). It is consistent with expectations from the near absence of energy barriers between the different states of C, T, O, and R at the phase convergence region. Furthermore, T glass-R glass transitions around $x = 3$–5 starting from this discovered glass convergence region remain relatively high permittivity (approximately 3050) and low permittivity hysteresis (0.7–1.2 K). This is higher than the ambient or low-temperature performance of many state-of-the-art lead or lead-free piezoelectrics [7,35]. In the composition region of $x = 6$–7, this T glass-R glass transition exhibits a relatively high permittivity value (2800) but a large thermal hysteresis of permittivity (approximately 7 K), which may be induced by freezing of domain walls, decreasing the domain size due to the high dopant level. For $x = 1$, it exhibits anomalously higher permittivity (approximately 3200) and the highest hysteresis (approximately 11 K). It is proved to be true for several times and may be attributed to the FE-relaxor crossover region.

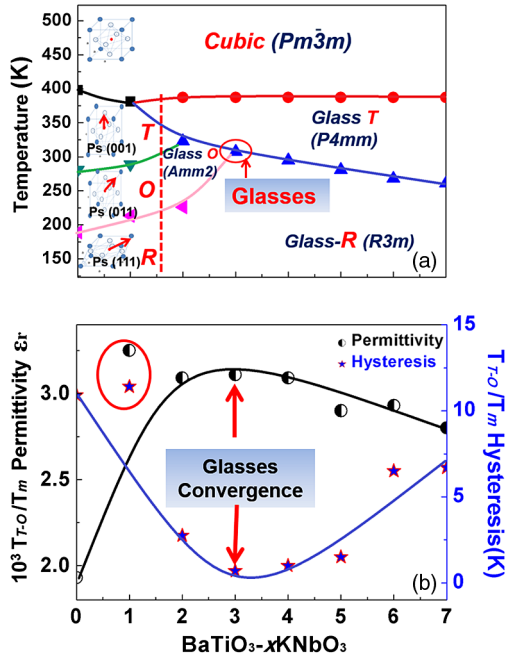

FIG. 5. (a) Phase diagram of BT-xKN ceramics. (b) The value of dielectric permittivity (black and white markers line, left axis) and thermal hysteresis (blue star line, right axis) of permittivity around the temperature $T_{t\text{-}o}/T_m$ in BT-xKN with composition $x = 0$–7, which reveals one state convergence region: the glass coexistence region ($x = 3$).

The discovered low hysteresis with remaining high dielectric permittivity (proportional to the high electrical capacity Cp) indicates that the glass state can respond to an external electrical stimulus sensitively and fast in a wide frequency and temperature range. This may have potential applications, for instance, electric energy-storage capacitors. The schematic diagram for the energy-storing process in ferroelectrics is shown in Fig. 6(a). The green part shows storing the energy density under an external electrical field. It is clear that low P_r and high P_m are required in order to improve the energy-storage density of ferroelectrics. From Figs. 6(b) and 6(c), the relatively high P_m (2.5–3.5 $\mu C/cm^2$) and extremely low P_r (0.1–0.2 $\mu C/cm^2$) of BT-2KN and BT-3KN ceramics under a 1 kV/mm electrical field are observed over a wide temperature range of 220–350 K (diffusion T glass-O-R glass transition regions). Therefore, our work may suggest a way to improve the performance of energy-storage capacitors with high storing density and good thermal stability.

In order to understand the glass-glass transitions with the characteristics of morphotropic phase boundaries, simulations are carried out for a single crystal in 2D which includes a first-order cubic → tetragonal → orthorhombic ferroelectric transition in $BaTiO_3$. The total free energy of the system includes the following three physically distinctive terms [36–38]:

$$\begin{aligned} F &= F(p,\bar{c}) + F(p,\varphi) + F(p) \\ &= \int_V f_{\text{bulk}} dV + \int_V f_{\text{couple}} dV \\ &\quad + \int_V (f_{\text{elas}} + f_{\text{elec}} + f_{\text{grad}}) dV. \end{aligned} \tag{1}$$

The first term describes the bulk free energy density f_{bulk}, which is expressed by the Landau free energy term,

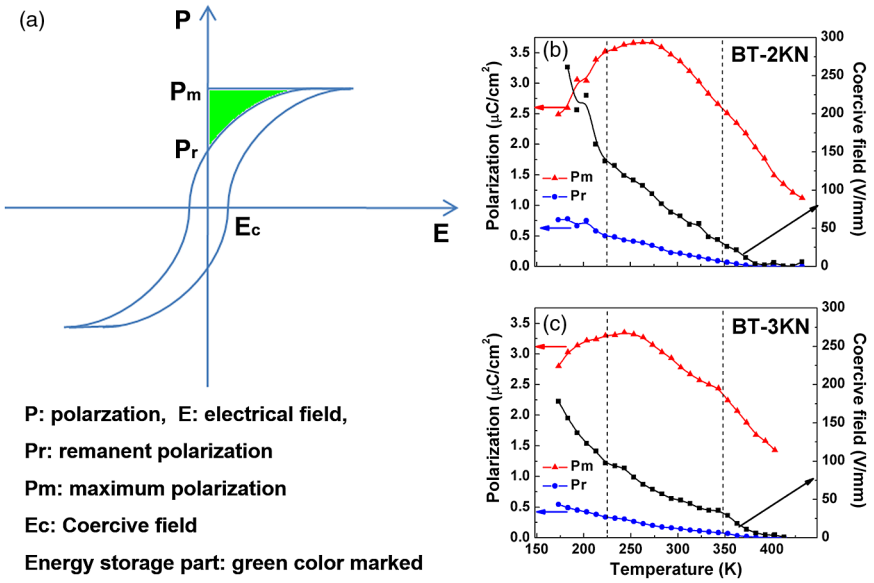

FIG. 6. (a) The schematic picture of the energy-storage effect of ferroelectrics, (b) the temperature evolution of P_m, P_r, and E_c in BT-2KN, and (c) the temperature vs P_m, P_r, and E_c properties in BT-3KN, low P_r, and relative high P_m under a wide temperature range suggests the good thermal stability of the energy-storage effect.

the related Landau coefficients, and polynomial used in our simulations to describe a phase transition in pure BT is from Li *et al.* [38]. The second term describes the dipole effect caused by doped point defects, e.g., KN, where $f_{\text{couple}} = -\int d^3x \sum_i^3 P_i(\mathbf{x}) \cdot \boldsymbol{\varphi}_{\text{loc}}(\mathbf{x})$, and $\boldsymbol{\varphi}_{\text{loc}}(\mathbf{x})$ are dipolar fields (local polarization field) created by the point defects [36,39]. $\boldsymbol{\varphi}_{\text{loc}}(\mathbf{x})$ is assumed to distribute randomly at the cubic matrix and does not change under cooling. The last integral in Eq. (1) includes the long-range elastic and electrostatic interaction energies and the short-range exchange interaction energy. The temporal evolution of the spontaneous polarization field can be obtained by solving the time-dependent Ginzburg-Landau equation: $\frac{dP_i(\mathbf{x},t)}{dt} = -M\frac{\delta F}{\delta P_i(\mathbf{x},t)}$, $i = 1, 2, 3$. The domain structure is described by a distribution of spontaneous polarization $P = (P1, P2, P3)$.

Based on this model, the formation of acceptor-donor percolating electric dipoles networks at high KN-doped $BaTiO_3$ (2% KN) is calculated. The acceptor dopant has a lower valance than the substituted ions in the matrix, e.g., K^+ substituting Ba^{2+}. The donor dopant has a higher electrovalence than the substituted ions in the matrix, e.g., Nb^{5+} substituting Ti^{4+}. So, the doping of K^+ and Nb^{5+} will produce static local acceptor-donor electric dipole. The detailed evolution process can be seen in the phase field simulation of Fig. 7. Figures 7(a)–7(d) and 7(a')–7(d') show the evolution of dipoles upon cooling above T_c (before the formation of spontaneous polarization). Static dipoles caused by dopants [Figs. 7(a) and 7(a')] will induce more dipoles [Figs. 7(b)–7(d) and 7(b')–7(d')] around itself upon cooling due to the electrostatic force. With the increase of induced dipoles, the system will form such a dipole network structure [Figs. 7(d) and 7(d')]. The acceptor-donor percolating electric dipole network will produce a confinement in the system and limit the growth of ferroelectric domains upon further cooling.

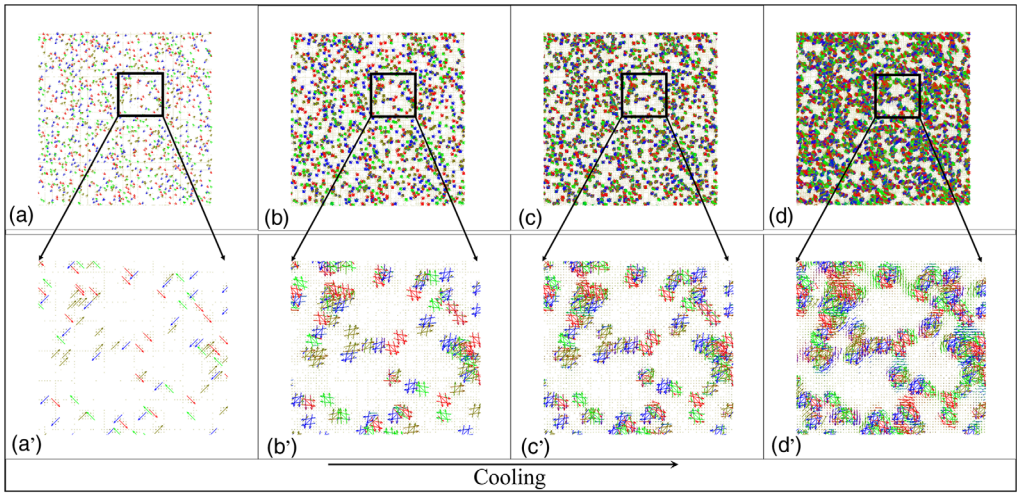

FIG. 7. The evolution of an acceptor-donor percolating electric dipole network at high doped BT (2% KN). (a)–(d) describe the formation of a dipole network upon cooling. (a')–(d') exhibit the enlarged area in (a)–(d). Arrows and colors describe different dipole vectors.

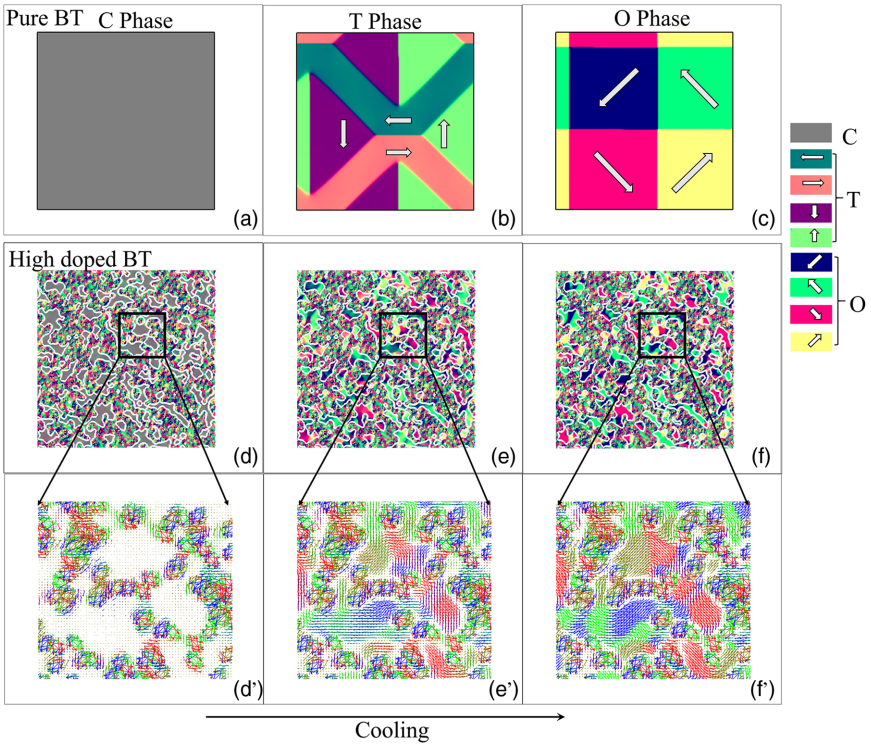

FIG. 8. Calculated microstructural evolution of pure BT (a)–(c) and high doped BT (i.e., 2%kN) (d)–(f) and enlarged microstructures (d')–(f') upon cooling in 2D. The white line in high doped BT describes the network caused by a local dipolar field from doping. Arrows and colors describe the polarization direction.

Based on the "acceptor-donor percolating electric dipole network" model, the microstructural evolutions of the pure $BaTiO_3$ and high dipole-doped $BaTiO_3$ are described, as shown in Fig. 8. For pure $BaTiO_3$, the microstructure picture of high temperature is shown in Fig. 8(a), where the cubic phase (gray color) is the stable phase. With temperature decreasing, the spontaneous ferroelectric transitions of *C-T* and *T-O* occur consequently. The microdomain patterns of the tetragonal phase and the orthorhombic phase are shown in Figs. 8(b) and 8(c), respectively. As a comparison, the microstructure evolution of the high K-Nb dipole-doped $BaTiO_3$ is shown in Figs. 8(d)–8(f). Its microstructure at a high temperature [Fig. 8(d)] shows that the distributed defect dipoles will produce an acceptor-donor percolating dipole network in order to make the electric energy of the system lower. Consequently, the system will be frustrated to nano *T*, nano *O*, and nano *R* glass structures upon cooling, as shown in the white lines in Figs. 8(d)–8(f). Figures 8(d')–8(f') show enlarged microstructures with arrows, which show the transition process clearly in a small scale. Because of the glass transition characteristics, there exists a large temperature region where the different structures coexist (local *C*, local *T*, and local *O*), which could be the physical origin of glass-glass transitions and unique properties. This PEDN can also be evidenced by Raman data shown as Figs. 4(b) and 4(d). Above the dip of the *C-T* glass transition of BT-2KN, the phonon vibration starts to soften and then hardens upon cooling from 473 K, for both the LO and TO modes. This phenomenon is completely different with the BTO case, which just shows softening from 473 K to the *C-T* transition. It is considered as the evidence for the formation of PEDN structure by KN doping.

V. CONCLUSION

Glass-glass transitions are discovered in KN(K^+/Nb^{5+})-doped $BaTiO_3$ lead-free ferroelectric ceramics, which can effectively achieve a small thermal hysteresis (approximately 1.0 K) with a large dielectric constant (approximately 3000), small remanent polarization P_r, and large maximum polarization P_m over a wide temperature range (220–350 K). Our phase field simulations find that this glass-glass transition can be understood by the formation of an acceptor-donor percolating electric dipole network. This work may stimulate the research in the fundamental theory of glass-glass transitions in ferroic materials and shed light on the design of energy-storage devices with a high dielectric permittivity, low hysteresis loss, and wide temperature range.

ACKNOWLEDGMENTS

The authors gratefully acknowledge the funding support of the China Scholarship Council No. 201506280034, the National Basic Research Program of China (Grants No. 2016YFB0701302 and No. 2014CB644003), National Natural Science Foundation of China (Grants No. 51671156, No. 51772238, No. 51431007, and No. 51321003), as well as the Project of the Chinese Academy of Engineering Physics (Grant No. YK2015-0602006), and the Natural

Environment Research Council and the Engineering and Physical Sciences Research Council of Great Britain (Grants No. NE/B505738/1, No. NE/F017081/1, and No. EP/I036079/1).

[1] Q. Burlingame, S. Wu, M. Lin, and Q. M. Zhang, Conduction mechanisms and structure-property relationships in high energy density aromatic polythiourea dielectric films, Adv. Energy Mater. **3**, 1051 (2013).

[2] B. Chu, X. Zhou, K. Ren, B. Neese, M. Lin, Q. Wang, F. Bauer, and Q. M. Zhang, A dielectric polymer with high electric energy density and fast discharge speed, Science **313**, 334 (2006).

[3] X. Hao, J. Zhai, B. K. Ling, and Z. Xu, A comprehensive review on the progress of lead zirconate-based antiferroelectric materials, Prog. Mater. Sci. **63**, 1 (2014).

[4] L. Zhao, Q. Liu, S. Zhang, and J. F. Li, Lead-free $AgNbO_3$ anti-ferroelectric ceramics with an enhanced energy storage performance using MnO_2 modification, J. Mater. Chem. C **4**, 8380 (2016).

[5] T. M. I. Mahlia, T. J. Saktisahdan, A. Jannifar, M. H. Hasan, and H. S. C. Matseelar, A review of available methods and development on energy storage; technology update, Renewable Sustainable Energy Rev. **33**, 532 (2014).

[6] Z. Yao, Z. Song, H. Hao, Z. Yu, M. Cao, S. Zhang, M. T. Lanagan, and H. Liu, Homogeneous/inhomogeneous-structured dielectrics and their energy-storage performances, Adv. Mater. **29**, 1601727 (2017).

[7] T. R. Shrout and S. J. Zhang, Lead-free piezoelectric ceramics: Alternatives for PZT?, J. Electroceram. **19**, 113 (2007).

[8] A. A. Bokov and Z.-G. Ye, in *Frontiers of Ferroelectricity: A Special Issue of the Journal of Materials Science* (Springer, Boston, MA, 2007).

[9] H. Wang, J. Zhu, N. Lu, A. A. Bokov, Z.-G. Ye, and X. W. Zhang, Hierarchical micro-/nanoscale domain structure in M_C phase of $(1\text{-}x)Pb(Mg_{1/3}Nb_{2/3})O3\text{-}xPbTiO_3$ single crystal, Appl. Phys. Lett. **89**, 042908 (2006).

[10] A. A. Bokov and Z.-G. Ye, Domain structure in the monoclinic Pm phase of $Pb(Mg_{1/3}Nb_{2/3})O_3$-$PbTiO_3$ single crystals, J. Appl. Phys. **95**, 6347 (2004).

[11] F. Bai, J. Li, and D. Viehland, Domain hierarchy in annealed (001)-oriented $Pb(Mg_{1/3}Nb_{2/3})O_3$-x%$PbTiO_3$ single crystals, Appl. Phys. Lett. **85**, 2313 (2004).

[12] X. Hao, Y. Wang, L. Zhang, L. Zhang, and S. An, Composition-dependent dielectric and energy-storage properties of $(Pb, La)(Zr, Sn, Ti)O_3$ antiferroelectric thick films, Appl. Phys. Lett. **102**, 192901 (2013).

[13] K. Binder and W. Kob, *Glassy Materials and Disordered Solids: An Introduction to their Statistical Mechanics* (World Scientific, Singapore, 2011).

[14] X. Ren, Y. Wang, K. Otsuka, P. Lloveras, T. Castán, M. Porta, A. Planes, and A. Saxena, Ferroelastic nanostructures and nanoscale transitions: Ferroics with point defects, MRS Bull. **34**, 838 (2009).

[15] X. Ren, Y. Wang, Y. Zhou, Z. Zhang, D. Wang, G. Fan, K. Otsuka, T. Suzuki, Y. Ji, and J. Zhang, Strain glass in ferroelastic systems: Premartensitic tweed versus strain glass, Philos. Mag. **90**, 141 (2010).

[16] G. A. Rossetti, A. G. Khachaturyan, G. Akcay, and Y. Ni, Ferroelectric solid solutions with morphotropic boundaries: Vanishing polarization anisotropy, adaptive, polar glass, and two-phase states, J. Appl. Phys. **103**, 114113 (2008).

[17] M. Ahart, M. Somayazulu, R. E. Cohen, P. Ganesh, P. Dera, H.-k. Mao, R. J. Hemley, Y. Ren, P. Liermann, and Z. Wu, Origin of morphotropic phase boundaries in ferroelectrics, Nature (London) **451**, 545 (2008).

[18] B. Noheda, D. E. Cox, G. Shirane, J. A. Gonzalo, L. E. Cross, and S.-E. Park, A monoclinic ferroelectric phase in the $Pb(Zr_{1-x}Ti_x)O_3$ solid solution, Appl. Phys. Lett. **74**, 2059 (1999).

[19] A. Khachaturyan, Ferroelectric solid solutions with morphotropic boundary: Rotational instability of polarization, metastable coexistence of phases and nanodomain adaptive states, Philos. Mag. **90**, 37 (2010).

[20] D. Damjanovic, A morphotropic phase boundary system based on polarization rotation and polarization extension, Appl. Phys. Lett. **97**, 062906 (2010).

[21] R. Theissmann, L. A. Schmitt, J. Kling, R. Schierholz, K. A. Schönau, H. Fuess, M. Knapp, H. Kungl, and M. J. Hoffmann, Nanodomains in morphotropic lead zirconate titanate ceramics: On the origin of the strong piezoelectric effect, J. Appl. Phys. **102**, 079902 (2007).

[22] B. Noheda and D. E. Cox, Bridging phases at the morphotropic boundaries of lead oxide solid solutions, Phase Transitions **79**, 5 (2006).

[23] R. Bratton and T. Tien, Phase transitions in the system $BaTiO_3$-$KNbO_3$, J. Am. Ceram. Soc. **50**, 90 (1967).

[24] Z. Sun, D. Xue, H. Wu, Y. Ji, X. Ding, D. Wang, Y. Yang, and X. Ren, Time-dependent ferroelectric transition in $Pb_{(1-x)}(Zr_{0.4}Ti_{0.6})_{(1-x/4)}O_3 - x$La system, Appl. Phys. Lett. **102**, 222907 (2013).

[25] S. Sarkar, X. Ren, and K. Otsuka, Evidence for Strain Glass in the Ferroelastic-Martensitic System $Ti50\text{-}xNi50 + x$, Phys. Rev. Lett. **95**, 205702 (2005).

[26] M. Carpenter, Static and dynamic strain coupling behaviour of ferroic and multiferroic perovskites from resonant ultrasound spectroscopy, J. Phys. Condens. Matter **27**, 263201 (2015).

[27] J. Schiemer, M. A. Carpenter, D. M. Evans, J. M. Gregg, A. Schilling, M. Arredondo, M. Alexe, D. Sanchez, N. Ortega, R. S. Katiyar, M. Echizen, E. Colliver, S. Dutton, and J. F. Scott, Studies of the room-temperature multiferroic $Pb(Fe_{0.5}Ta_{0.5})_{0.4}(Zr_{0.53}Ti_{0.47})_{0.6}O_3$: Resonant ultrasound spectroscopy, dielectric, and magnetic phenomena, Adv. Funct. Mater. **24**, 2993 (2014).

[28] E. K. H. Salje, M. A. Carpenter, G. F. Nataf, G. Picht, K. Webber, J. Weerasinghe, S. Lisenkov, and L. Bellaiche, Elastic excitations in $BaTiO_3$ single crystals and ceramics: Mobile domain boundaries and polar nanoregions observed by resonant ultrasonic spectroscopy, Phys. Rev. B **87**, 014106 (2013).

[29] R. E. A. McKnight, M. A. Carpenter, T. W. Darling, A. Buckley, and P. A. Taylor, Acoustic dissipation associated with phase transitions in lawsonite, $CaAl_2Si_2O_7(OH)_2 \cdot H_2O$, Am. Mineral. **92**, 1665 (2007).

[30] L. Zhang, X. Ren, and M. A. Carpenter, Influence of local strain heterogeneity on high piezoelectricity in

$0.5Ba(Zr_{0.2}Ti_{0.8})O_3$-$0.5(Ba_{0.7}Ca_{0.3})TiO_3$ ceramics, Phys. Rev. B **95**, 054116 (2017).

[31] L. Zhang, M. Zhang, L. Wang, C. Zhou, Z. Zhang, Y. Yao, L. Zhang, D. Xue, X. Lou, and X. Ren, Phase transitions and the piezoelectricity around morphotropic phase boundary in $Ba(Zr_{0.2}Ti_{0.8})O_3$-$x(Ba_{0.7}Ca_{0.3})TiO_3$ lead-free solid solution, Appl. Phys. Lett. **105**, 162908 (2014).

[32] P. S. Dobal, A. Dixit, R. S. Katiyar, Z. Yu, R. Guo, and A. S. Bhalla, Micro-Raman scattering and dielectric investigations of phase transition behavior in the $BaTiO_3$-$BaZrO_3$ system, J. Appl. Phys. **89**, 8085 (2001).

[33] B. Jannot, L. Gnininvi, and G. Godefroy, Symmetry problems on raman scattering by pure and doped $BaTiO_3$ in the cubic phase, Ferroelectrics **37**, 669 (1981).

[34] C. H. Perry and D. B. Hall, Temperature Dependence of the Raman Spectrum of $BaTiO_3$, Phys. Rev. Lett. **15**, 700 (1965).

[35] W. Liu and X. Ren, Large Piezoelectric Effect in Pb-Free Ceramics, Phys. Rev. Lett. **103**, 257602 (2009).

[36] D. Wang, X. Q. Ke, Y. Z. Wang, J. H. Gao, Y. Wang, L. X. Zhang, S. Yang, and X. B. Ren, Phase diagram of polar states in doped ferroelectric systems, Phys. Rev. B **86**, 054120 (2012).

[37] S. Semenovskaya and A. G. Khachaturyan, Development of ferroelectric mixed states in a random field of static defects, J. Appl. Phys. **83**, 5125 (1998).

[38] Y. L. Li, L. E. Cross, and L. Q. Chen, A phenomenological thermodynamic potential for $BaTiO_3$ single crystals, J. Appl. Phys. **98**, 064101 (2005).

[39] A. P. Levanyuk and A. S. Sigov, edited by G. W. Taylor and L. A. Shuvalov, *Defects and Structural Phase Transitions*, Ferroelectricity and related phenomena Vol. 6 (Gordon and Breach, New York, 1988).